TUM SCHOOL OF COMPUTATION, INFORMATION AND TECHNOLOGY (CIT)

TECHNICAL UNIVERSITY OF MUNICH

Report Submitted to Praktikum Robot Modelling and Identification (IN2106)

# Experiment 7: Implementation of an Impedance Controller for a 2-Link Planar Arm

Jesus Arturo Sol Navarro, Sarah Weber, Zhenyi Xu

TECHNICAL UNIVERSITY OF MUNICH

Report Submitted to Praktikum Robot Modelling and Identification
(IN2106)

# Experiment 7: Implementation of an Impedance Controller for a 2-Link Planar Arm

| | |
|---|---|
| Author: | Jesus Arturo Sol Navarro, Sarah Weber, Zhenyi Xu |
| Lecturers: | Prof. Dr. M.Sc. Alexander König, M.Sc. Moritz Eckhoff, Moein Forouhar |
| Submission Date: | July 3, 2025 |

We confirm that this report is my our own work and we have documented all sources and material used.

Munich, July 3, 2025
Jesus Arturo Sol Navarro, Sarah Weber, Zhenyi Xu

# Contents

# 1 ICR - Implementation of an Impedance Controller for a 2-Link Planar Arm

The objective of this experiment is to implement an impedance controller for 2-link robot arm, shown in Fig. 1.1. The parameters of the robot link used in this experiment are summarized in Table 1.1.

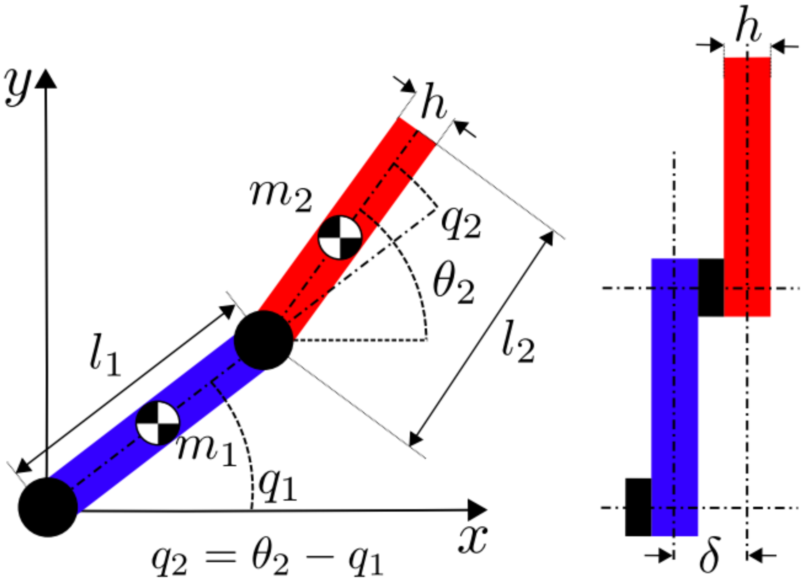

Figure 1.1: Sketch of the robot link.

| Parameter | Description | Value | Unit |
|---|---|---|---|
| $m_1, m_2$ | Mass of the links | 1 | Kg |
| $l_1, l_2$ | Lever arm of the link1/link2 | 1 | m |

Table 1.1: System parameters

## 1.1 Task 1

In this task, gravity compensation is implemented for the 2-link robot arm. The initial joint configuration is set to $q_0 = [0,\ 0]^\top$ rad. An external torque of $[0.5\ 3.0]^\top$ Nm is applied to the robot arm for a duration of 0.2 seconds, starting at $t = 5$ s.

As observed in Figure 1.2, the joint angles deviate from their initial positions in response to the torque input. After the torque is removed, the angles do not return exactly to zero, indicating a steady-state error in the system. This shows that the current controller does not fully reject the disturbance .

.

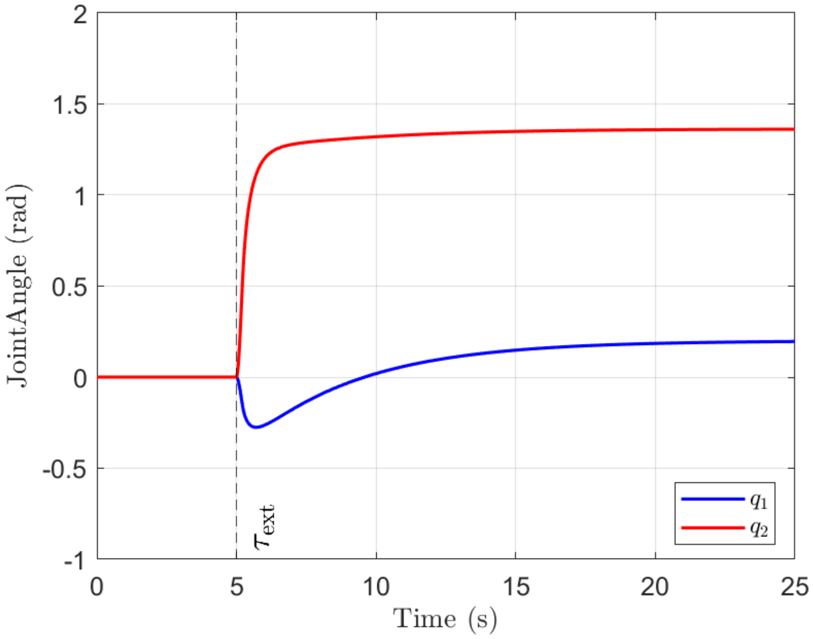

Figure 1.2: Joint angle response of the 2-link robot arm after applying external torque under gravity compensation.

## 1.2 Task 2

In this task, joint-level impedance-based control strategies are implemented and analyzed. Three copies of the given 2-link robot arm are simulated in parallel, each controlled independently to reach the joint angle reference $\mathbf{q}_d = [0.25,\ 0.4]^\top$ rad. The initial joint configuration is set to $q_0 = [0,\ 0]^\top$ rad. The primary objective is to ensure accurate tracking while minimizing overshoot and oscillations.

### (a)

In this subtask, an impedance-based controller of the form $F = K\Delta q$ is implemented, where $K$ is the stiffness matrix and $\Delta q$ is the position error between the desired and actual joint angles. The same stiffness value $K$ was applied to both joints. **Friction in the robot arm model is set to zero.**

Figure 1.3 shows that increasing the stiffness gain $K$ leads to more frequent oscillations in the joint angle response. This behavior is expected, as a higher stiffness introduces a stronger restoring force.

On the other hand, since friction was disabled in the model, no energy dissipation was present. As a result, the system did not settle to a steady state but continued to oscillate indefinitely. However, when gravity compensation was enabled, the system oscillated around the desired joint position, demonstrating that compensation effectively shifted the equilibrium to the desired joint angles, even if perfect convergence was not achieved.

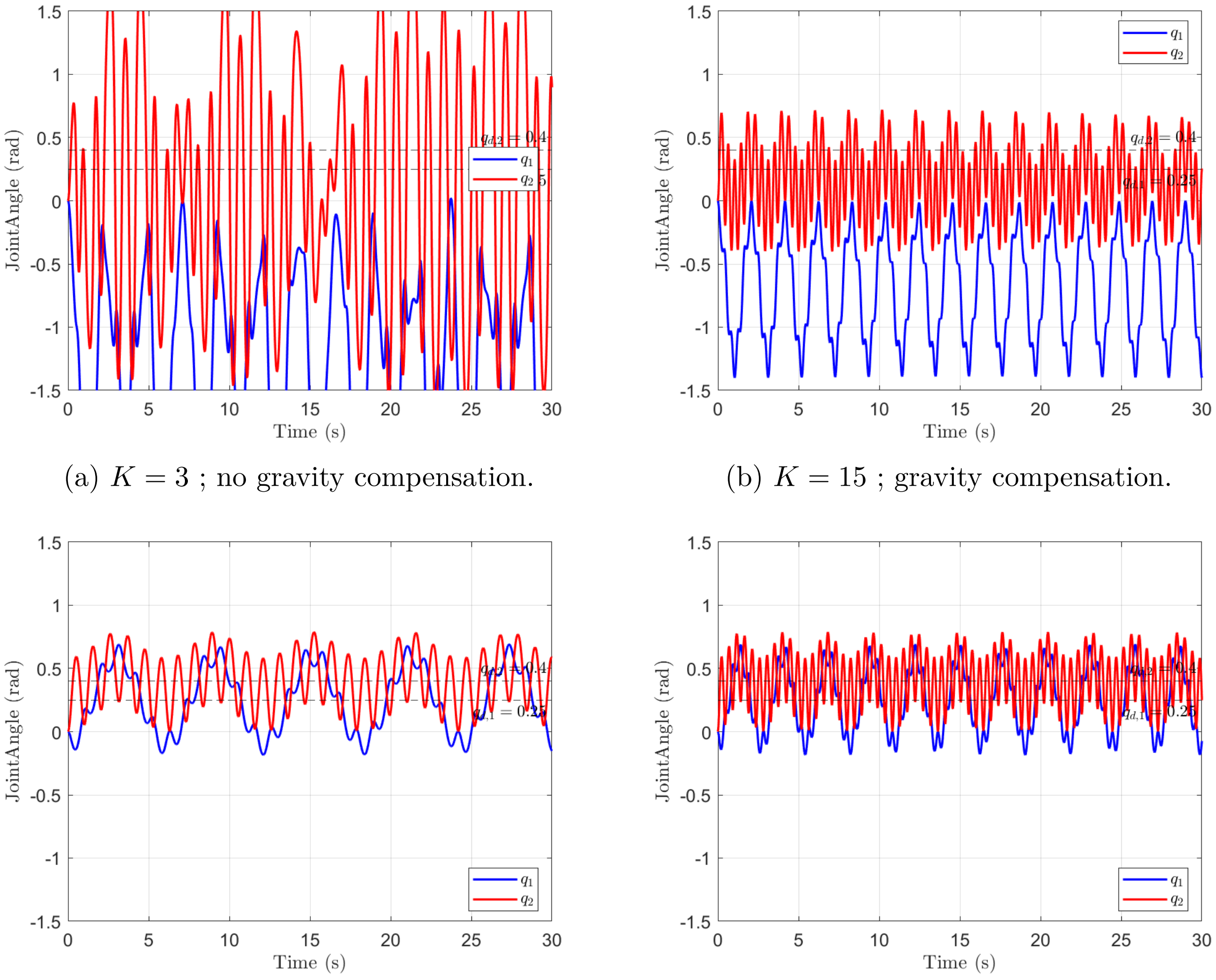

(a) $K = 3$ ; no gravity compensation.

(b) $K = 15$ ; gravity compensation.

(c) $K = 3$ ; gravity compensation.

(d) $K = 15$ ; gravity compensation.

Figure 1.3: Joint angle responses under different stiffness values $(K)$, with and without gravity compensation.

## (b)

In this subtask, an impedance-based controller of the form $F = K\Delta q$ is implemented. The same stiffness value $K$ is applied to both joints. **Friction in the robot arm model is enabled, while gravity compensation is disabled** .

Figure 1.4 shows that increasing the stiffness gain $K$ leads to higher oscillation frequency .The joints get closer to the desired angles with less steady-state error, but this comes with more rapid oscillations. While higher $K$ improves accuracy, it also makes the system more sensitive and less smooth. A trade-off between precision and stability becomes noticeable.

Friction in the model helps dissipate energy over time, allowing the system to eventually settle. Without it, the oscillations would continue indefinitely.

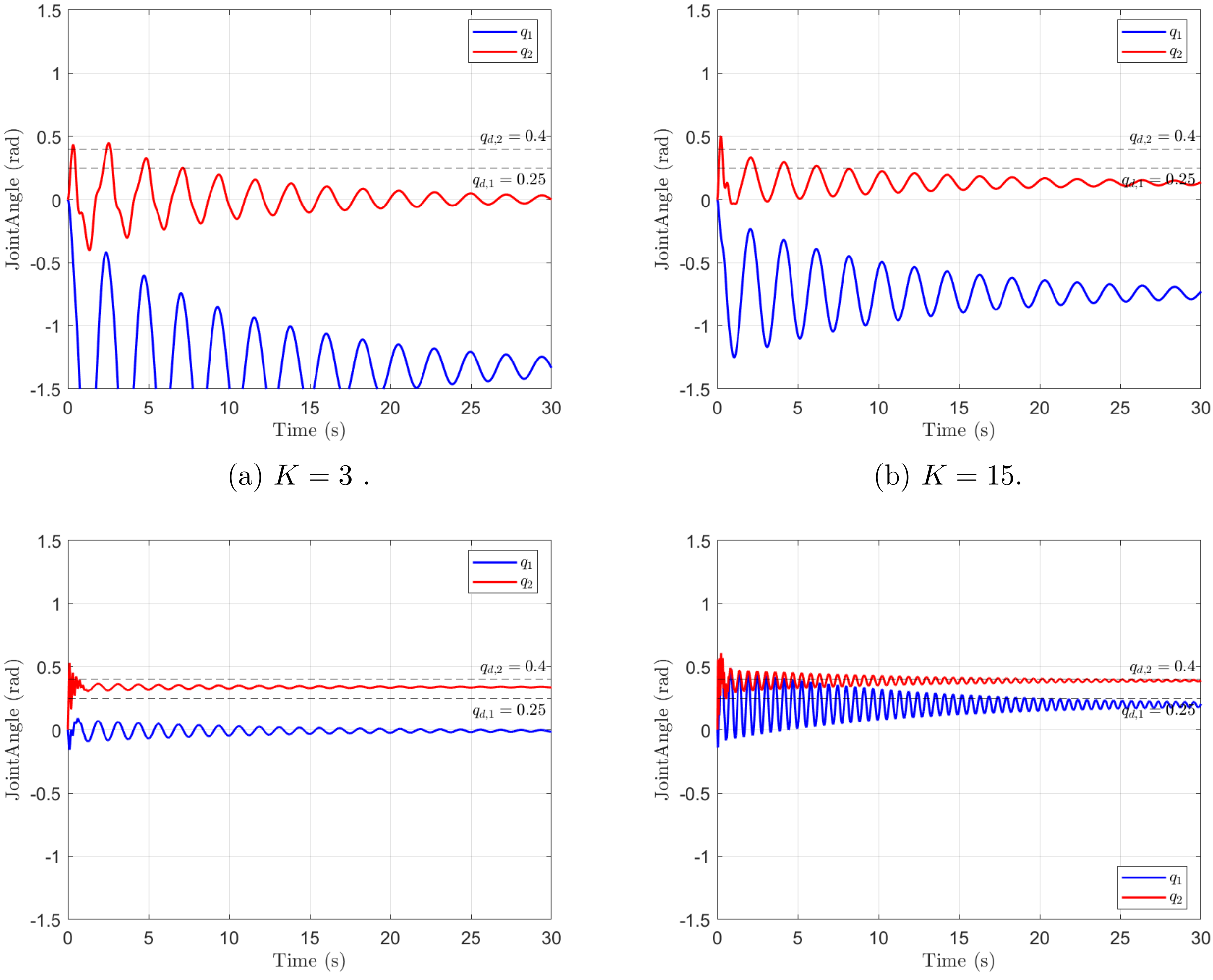

(a) $K = 3$ .

(b) $K = 15$.

(c) $K = 75$ .

(d) $K = 375$ .

Figure 1.4: Joint angle responses under different stiffness values ($K$), gravity disabled and friction enabled.

## (c)

In this subtask, an impedance-based controller of the form $F = K\Delta q + D\Delta\dot{q}$ is implemented. The same stiffness value $K$ and damping value $D$ are applied to both joints. **Friction in the robot arm model and gravity compensation are enabled** .

Figure 1.5 illustrates the effect of different damping values $D$ on the joint angle response, with stiffness held constant at $K = 15$. When no damping is applied ($D = 0$), the system exhibits sustained oscillations due to the absence of energy dissipation. Introducing a small damping value ($D = 3$) results in an underdamped response with reduced oscillations and faster convergence. With $D = 12$, the system becomes critically damped, reaching the target without overshoot. At high damping ($D = 50$), the response is overdamped—stable but slow to settle.

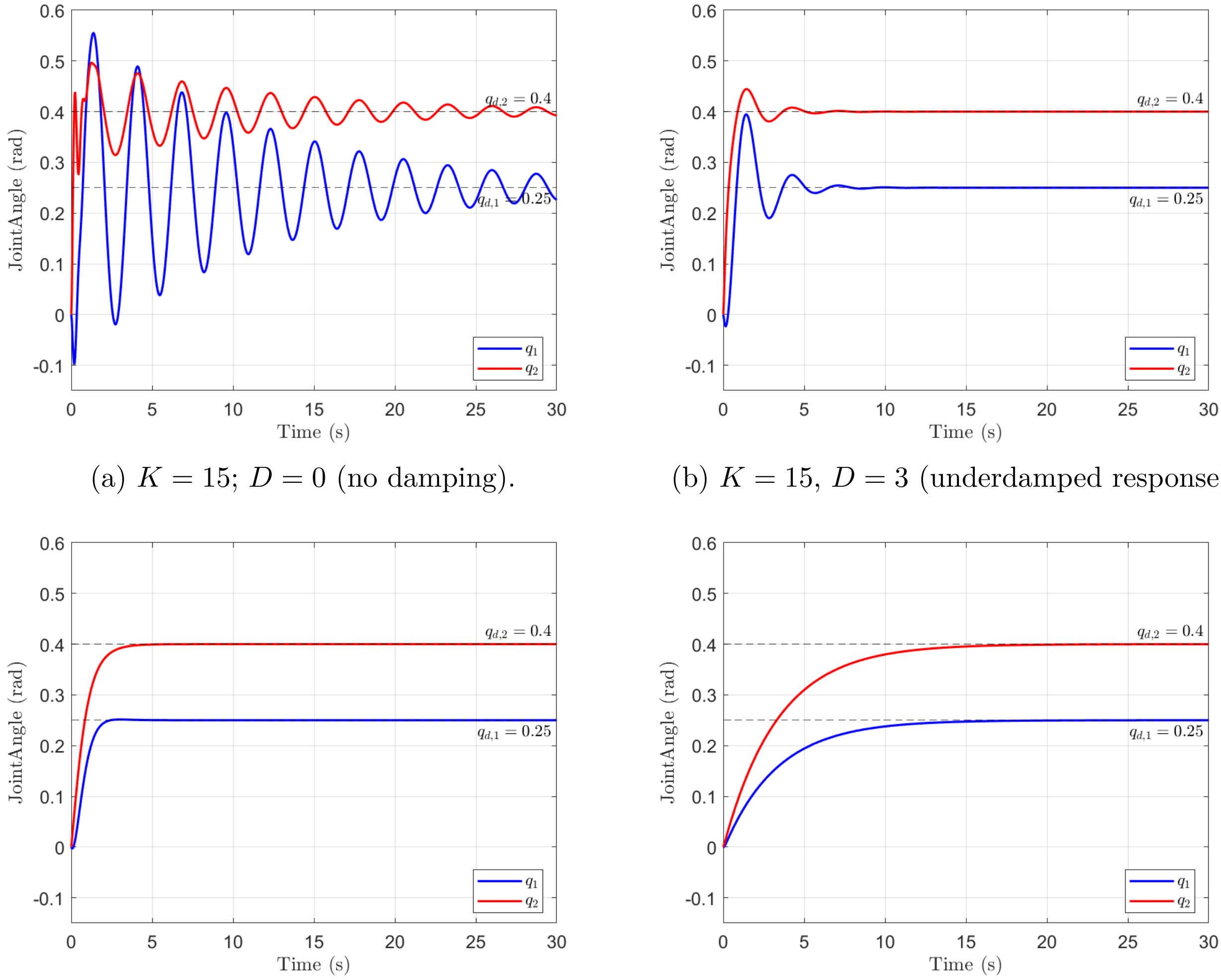

(a) $K = 15$; $D = 0$ (no damping).

(b) $K = 15$, $D = 3$ (underdamped response).

(c) $K = 15$, $D = 12$ (critically damped response).

(d) $K = 15$, $D = 50$ (overdamped response).

Figure 1.5: Joint angle responses under constant stiffness value ($K$) and different damping values ($D$), gravity compensation and friction enabled.

## Comparison of the systems

Across the three systems, different combinations of friction, gravity compensation, stiffness, and damping were tested to evaluate their impact on system behavior, as summarized in Table 1.2. In Subtask (a), the absence of both friction and damping led to continuous oscillations. Gravity compensation improved performance slightly by shifting the equilibrium to the correct target, but without energy dissipation, the system could not stabilize. In Subtask (b), enabling friction introduced natural damping, allowing the system to eventually settle. Higher stiffness values improved accuracy but increased oscillation frequency. Finally, in Subtask (c), artificial damping was introduced in addition to friction and gravity compensation. This allowed for more precise shaping of the response.

Table 1.2: Summary of simulation settings in each subtask.

| Subtask | Friction | Gravity Compensation | Control Law |
|---|---|---|---|
| (a) | Disabled | Both | $F = K\Delta q$ |
| (b) | Enabled | Disabled | $F = K\Delta q$ |
| (c) | Enabled | Enabled | $F = K\Delta q + D\Delta\dot{q}$ |

## 1.3 Task 3

For the given 2-link arm, the direct kinematics are implemented to convert joint angles into Cartesian coordinates. The goal is to compute the end-effector position $(x, y)$ and orientation $\theta_2$ based on the joint angles $q_1$ and $q_2$. The direct kinematics are given by:

$$\mathbf{x} = \begin{bmatrix} x \\ y \\ \theta_2 \end{bmatrix} = \begin{bmatrix} l_1 \cos(q_1) + l_2 \cos(q_1 + q_2) \\ l_1 \sin(q_1) + l_2 \sin(q_1 + q_2) \\ q_1 + q_2 \end{bmatrix}$$

To transform Cartesian forces applied at the tip of the second link into joint torques, the transposed Jacobian matrix is used:

$$\boldsymbol{\tau} = J^\top \mathbf{F}_{\text{cartesian}}$$

The Jacobian $J$ is derived from the direct kinematics of the end-effector position $(x, y)$ with respect to the joint angles $q_1$ and $q_2$. It is given by:

$$J = \frac{\partial x_i}{\partial q_j} = \begin{bmatrix} -l_1 \sin(q_1) - l_2 \sin(q_1 + q_2) & -l_2 \sin(q_1 + q_2) \\ l_1 \cos(q_1) + l_2 \cos(q_1 + q_2) & l_2 \cos(q_1 + q_2) \\ 1 & 1 \end{bmatrix}$$

This Jacobian corresponds to the tip of the second link, which is the point of interest for Cartesian control.

In the following, an impedance-based controller of the form

$$\mathbf{F} = \mathbf{K}\Delta\mathbf{x} + \mathbf{D}\Delta\dot{\mathbf{x}}$$

is implemented in Cartesian space. The stiffness matrix is defined as $\mathbf{K} = \text{diag}(k_x, k_y, k_\phi)$, and the damping matrix as $\mathbf{D} = \text{diag}(d_x, d_y, d_\phi)$, applied to regulate the Cartesian errors in position and orientation. The reference position is $x_s = \begin{bmatrix} 0.9 & 0.9 & 1.5708 \end{bmatrix}^T$, and the system starts from the initial state $\begin{bmatrix} 2 & 0 & 0 \end{bmatrix}^T$.

Figure 1.6 illustrates four different scenarios using Cartesian impedance control, where stiffness values are varied while maintaining a constant damping of $D = 10$ for all degrees of freedom:

- **Scenario a:** Equal stiffness in all directions ($k_x = k_y = k_\phi = 35$). Moderate control is achieved across position and orientation, but only y is regulated precisely.
- **Scenario b:** High stiffness in $x$ and $y$, low in orientation ($k_x = k_y = 35$, $k_\phi = 5$). Position tracking is accurate, while the end-effector orientation has a steady-state error.

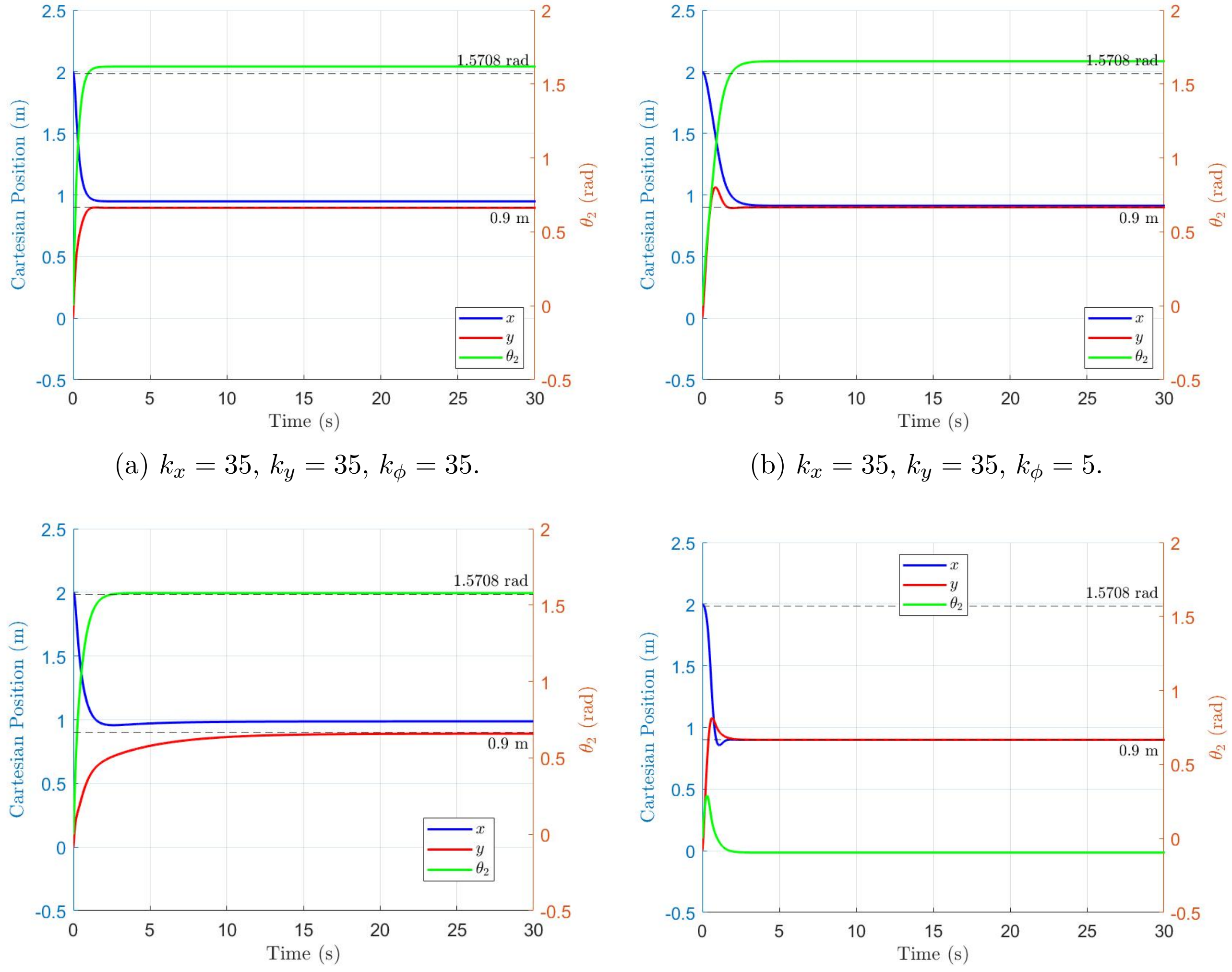

(a) $k_x = 35$, $k_y = 35$, $k_\phi = 35$.

(b) $k_x = 35$, $k_y = 35$, $k_\phi = 5$.

(c) $k_x = 3$, $k_y = 3$, $k_\phi = 35$.

(d) $k_x = 50$, $k_y = 50$, $k_\phi = 0$.

Figure 1.6: Cartesian coordinates responses under four different Cartesian stiffness configurations , with a constant damping value of $D = 10$ applied to all degrees of freedom.

- **Scenario c:** Low stiffness in $x$ and $y$, high in orientation ($k_x = k_y = 3$, $k_\phi = 35$). The controller maintains orientation better, but x shows steady-state error.
- **Scenario d:** Stiffness only in position ($k_x = k_y = 50$, $k_\phi = 0$). Strong position regulation is observed, while orientation is left uncontrolled .

In conclusion, due to the robot's limited actuation—only two joints available for three Cartesian degrees of freedom—it is not possible to minimize all errors simultaneously. The control effort must be distributed, for instance, by prioritizing position over orientation. This trade-off is clearly observed in the tested scenarios: when stiffness is increased in $x$ and $y$, the orientation error grows, and vice versa. Therefore, the controller must be carefully tuned to favor the most critical cartesian coordinates, depending on the application requirements.